Vol. 6, No. 1, February 2022, pp. 69–78

Current Optics and Photonics

Regular Paper

Research on Thermal Refocusing System of High-resolution Space Camera

Weiyan Li[1,2,3], Qunbo Lv[1,2,3]*, Jianwei Wang[1,2], Na Zhao[1,2,3], Zheng Tan[1,2,3], and Linlin Pei[1,2]

[1]*Aerospace Information Research Institute, Chinese Academy of Sciences, Beijng 100094, China*
[2]*Key Laboratory of Computational Optical Imagine Technology, Chinese Academy of Sciences, Beijing 100094, China*
[3]*School of Optoelectronics, University of Chinese Academy of Sciences, Beijing 100049, China*

(Received October 6, 2021 : revised November 29, 2021 : accepted December 20, 2021)

A high-resolution camera is a precise optical system. Its vibrations during transportation and launch, together with changes in temperature and gravity field in orbit, lead to different degrees of defocus of the camera. Thermal refocusing is one of the solutions to the problems related to in-orbit defocusing, but there are few relevant thermal refocusing mathematical models for systematic analysis and research. Therefore, to further research thermal refocusing systems by using the development of a high-resolution micro-nano satellite (CX6-02) super-resolution camera as an example, we established a thermal refocusing mathematical model based on the thermal elasticity theory on the basis of the secondary mirror position. The detailed design of the thermal refocusing system was carried out under the guidance of the mathematical model. Through optical–mechanical–thermal integration analysis and Zernike polynomial calculation, we found that the data error obtained was about 1%, and deformation in the secondary mirror surface conformed to the optical index, indicating the accuracy and reliability of the thermal refocusing mathematical model. In the final ground test, the thermal vacuum experimental verification data and in-orbit imaging results showed that the thermal refocusing system is consistent with the experimental data, and the performance is stable, which provides theoretical and technical support for the future development of a thermal refocusing space camera.

Keywords : High-resolution camera, Mathematical model, Secondary mirror, Thermal refocusing
OCIS codes : (120.4570) Optical design of instruments; (220.4830) Systems design; (230.0230) Optical devices; (260.0260) Physical optics

I. INTRODUCTION

A high-resolution camera is a kind of optical system with high accuracy. With the development of science and technology, both the reliability and accuracy of space cameras are required to be developed. However, due to fierce vibration in transportation and launch environments and the thermal vacuum environment in space, defocusing is inevitable, which would in turn leads to a decline in imaging quality. Defocusing may cause image quality degradation and lead to mission failure of the satellite. Therefore, in order to ensure high quality images, it is necessary to develop a refocusing system that is able to compensate for defocusing in orbit [1–4].

Most high-resolution cameras are coaxial Cassegrain, Ritchey–Chretien, or Korsch optical systems [5]. To solve in-orbit refocusing problems with minimum displacement of optical components, the most sensitive optical elements are preferred for focus compensation. The compensator element is generally a small secondary mirror for Casseg-

*Corresponding author: lvqb@aircas.ac.cn, ORCID 0000-0001-5343-2171

Color versions of one or more of the figures in this paper are available online.

pISSN: 2508-7266 / eISSN: 2508-7274 https://doi.org/10.3807/COPP.2022.6.1.069

rain/Korsch-type cameras. This secondary mirror is very sensitive, and small displacement of the mirror can provide good focus compensation [6]. In most of the literature, two methods are generally applied to space camera refocusing: mechanical refocusing and thermal refocusing. Mechanical refocusing is applied by controlling the movement of the secondary mirror with mechanical moving parts; for example, the HiRISE camera used a linear actuator to fine-tune its folding mirror [7], the secondary mirror of the Meteosat camera focused along the optical axis with a linear stepping motor [8], and ASTRO-F focused the secondary mirror position with a mechanical refocusing system [9]. Thermal refocusing is based on the controlled thermal expansion of mechanical components in designated directions [6], Pleiades-2 and SEOSAT cameras adjusted the position of the secondary mirror with a thermal refocusing mechanism along the optical axis [10, 11], and some space cameras are focused by adjusting the curvature of the secondary mirror through thermal control [6].

By researching the refocusing methods in the above literature, it is summarized that there are two major differences between the two generally adopted methods. The first difference is in volume and weight. Mechanical refocusing requires complex electromechanical systems such as a stepping motor, linear slide and brakes, and therefore the volume and weight have to be increased and the cost correspondingly increases; however, thermal refocusing systems are relatively simple and is mainly composed of a heater and temperature sensor, and the volume and weight required are relatively low. The second difference is reliability. Mechanical refocusing requires multiple moving parts to be accurately connected, so problems such as aging and being stuck may occur, while thermal refocusing is more reliable, since no joints, motors, brakes, etc., are required and no mechanism-related problems arise. With the development of science and technology, thermal refocusing technology tends to be mature and has been widely used. However, the mathematical model for thermal refocusing systems has yet to be systematically analyzed.

In order to research the thermal refocusing system of a high-resolution space camera, we took the development of a high-resolution micro-nano satellite (CX6-02) digital super-resolution camera as an example. The camera uses a typical Ritchey–Chretien optical system, and we selected the secondary mirror position for thermal refocusing. First, the mathematical model of a thermal refocusing system, based on thermoelastic theory, was established, and the thermal refocusing system was designed in detail with reference to the mathematical model. Then, to verify the accuracy of the mathematical model, the data were compared by Zernike polynomial calculation and optical–mechanical–thermal integration simulation analysis. Finally, ground experiment verification was carried out. The final experimental data and in-orbit imaging results show that the simulation data are very consistent with the experimental data, indicating that the structure has high stability under the guidance of the mathematical model of the thermal refocusing system.

II. OPTICAL DESIGN

The high-resolution digital satellite (CX6-02) camera is a typical Ritchey–Chretien optical system, as shown in Fig. 1(a), and is the most widely used and mature optical structure in high-resolution space camera systems. The camera is composed of an input window, through which the secondary mirror is suspended in the housing by means of a spider, a primary mirror, a calibration mirror group, and an optical sensor. As shown in Fig. 1(b), the designed camera has a 0.43 modulation transfer function (MTF) value, which is the theoretical limit of the optical design.

The primary mirror and secondary mirror are made of Zerodur, which is an optical material with expansion coefficient close to zero, to remove thermal expansions and contractions [12]. The physical specifications of the mirrors and the space camera parameter are listed in Table 1 and Table 2.

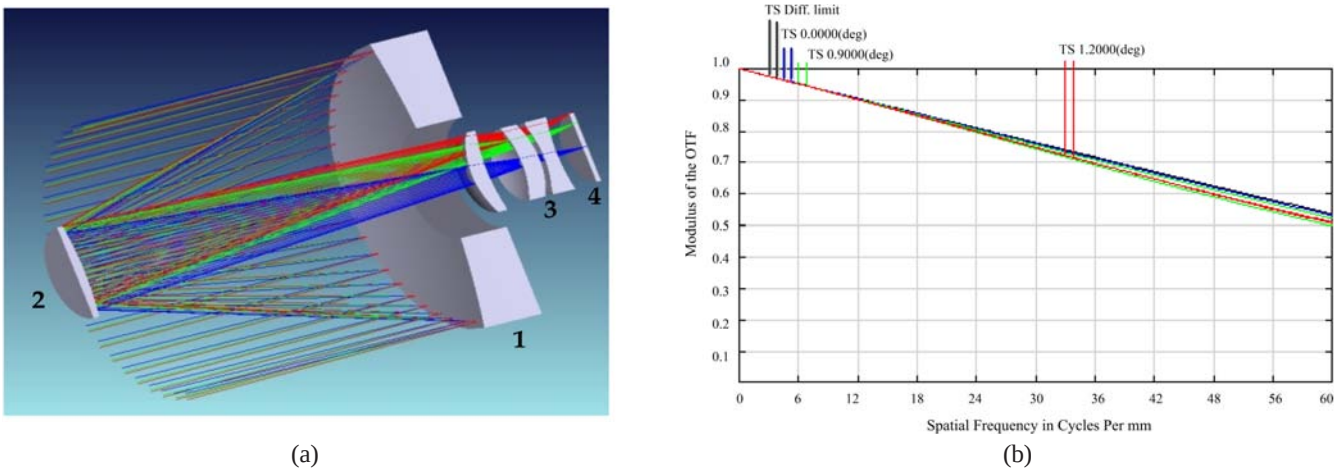

(a) (b)

FIG. 1. Schematic design of the Ritchey–Chretien camera: (a) optical system (1: primary mirror, 2: secondary mirror, 3: calibration mirror group, and 4: optical sensor) and (b) modulation transfer function (MTF) of the Ritchey–Chretien optical structure system.

In the processing and assembly of the optical system, the error sources mainly include mirror surface shape, off-center and tilt, mirror curvature radius, center thickness, Abbe number, etc. In order to research the impact of these errors on imaging quality, tolerance analysis of the camera was performed with Zemax optical design software (Zemax, WA, USA), and the sensitive error items were obtained, as shown in Table 3.

The tolerance analysis demonstrated that the camera design was far more sensitive to deformations along the optical axis than in other directions. Therefore, refocusing with sensitive factors is the most direct and effective method. Hence, we established a thermal refocusing system in the secondary mirror, since correcting the axial deformations of the camera structure with a refocusing system is necessary. However, the thermal deformation caused by refocusing will also affect the secondary mirror off-center, tilt and surface shape. Therefore, analyzing the influence of thermal deformation is a necessary process to ensure the reliability of the thermal refocusing system.

III. ESTABLISHING MATHEMATICAL MODEL

3.1. Structure of the Thermal Focusing System

We set the thermal refocusing system at the secondary mirror position, which ensured that the small displacement could achieve considerable focal length compensation. In order to achieve a larger displacement corresponding to a smaller temperature change, aluminum alloy with a high expansion coefficient should be selected as the thermal driver since it has relatively low energy consumption requirements [13].

In summary, the thermal refocusing system is shown in Fig. 2. and is composed of an aluminum ring, heaters, secondary mirror, secondary mirror support and temperature sensors.

The secondary mirror is connected to the secondary mirror support, then with the aluminum ring by trimming and assembled on the secondary mirror refocusing support with high precision. In the system, the thermal design is shown in Fig. 2. In order to improve the thermal uniform distribution accuracy, three heater-As are evenly distributed in the outer aluminum ring, and three temperature sensor-As are distributed between the heaters by changing the temperature of the heater-A to adjust the length of the aluminum ring for the purpose of refocusing. Heater-B is deployed outside the secondary mirror support to maintain the working temperature of the secondary mirror, while sensor-B is distributed in the inner and outer ring.

When we installed the secondary mirror thermal refocusing system, we used the primary mirror as the standard, and ensured that the tilt, off-center and distance between the secondary mirror met the optical design requirements through the trimming link.

3.2. Mathematical Model

The above thermal refocusing system is taken as the research object, and the mathematical model is established based on the thermal elasticity theory. In our analysis of the research object, we found that the structural form of the system was axisymmetric, and the structural deformation after a temperature change was axisymmetric [14]. The polar coordinates are determined by the polar diameter r, polar angle θ, and axial distance z. Figure 3 shows that ε is the positive strain and σ is the positive stress in the corresponding direction. Moreover, τ is shear stress in the corresponding direction.

According to Hooke's law, the equation is

$$\left.\begin{aligned}\frac{\partial \sigma_r}{\partial r}+\frac{\partial \tau_{zr}}{\partial z}+\frac{\sigma_r-\sigma_\theta}{r}=\\ \frac{\partial \sigma_z}{\partial z}+\frac{\partial \tau_{rz}}{\partial r}+\frac{\tau_{rz}}{r}=\end{aligned}\right\}. \tag{1}$$

TABLE 1. Space camera parameters

Parameter	Orbit Height (km)	Spectral Range (nm)	GSD (m)	Width (km)	Space Size (mm)
Performance	700	450–900	1.4	≥20	≤ø400 × 900

TABLE 3. Tolerance analysis

Type	Tolerance Value	MTF Value Changed
Distance Between Primary Mirror to Second	±0.001 mm	−0.02433267
Primary Mirror Off-center	±0.01 mm	−0.02427526
Second Mirror Off-center	±0.01 mm	−0.02427513
Primary Mirror Shape	λ/50	−0.01273267
Second Mirror Shape	λ/50	−0.01282743
Primary Mirror Tilt	±40″	−0.00852299
Second Mirror Tilt	±40″	−0.00852299
Mirror Curvature	±0.3 mm	−0.01390974

TABLE 2. Mirrors physical specifications

Parameter Type	Useful Zone (mm)	Mirror Shape	Material	Expansion coefficient 10^{-6}/°C	Weight (kg)
Primary Mirror	ϕ290	Concave Aspherical	Zerodur	0.05	4.5
Second Mirror	ϕ95	Convex Aspherical	Zerodur	0.05	0.3

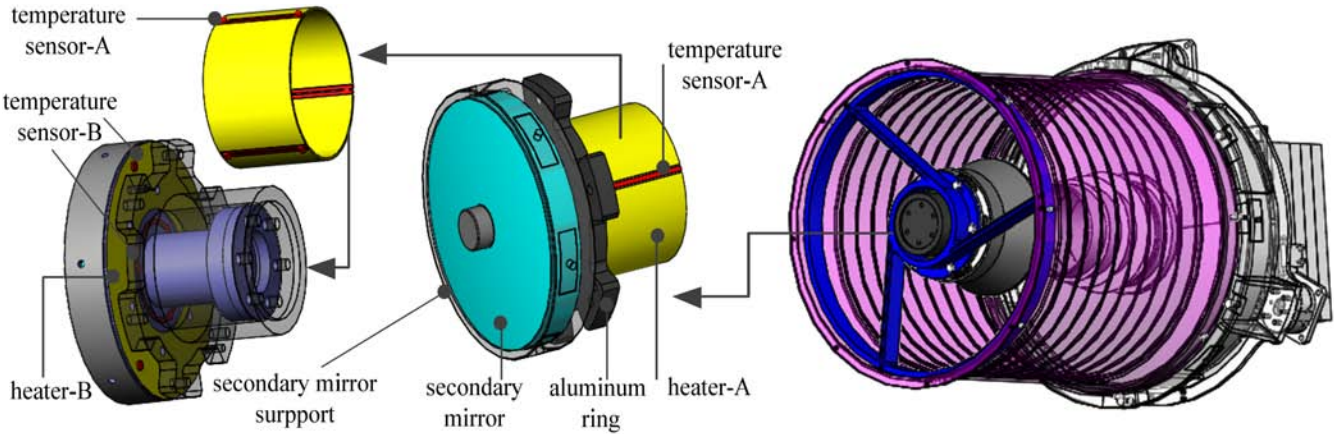

FIG. 2. Secondary mirror thermal refocusing system.

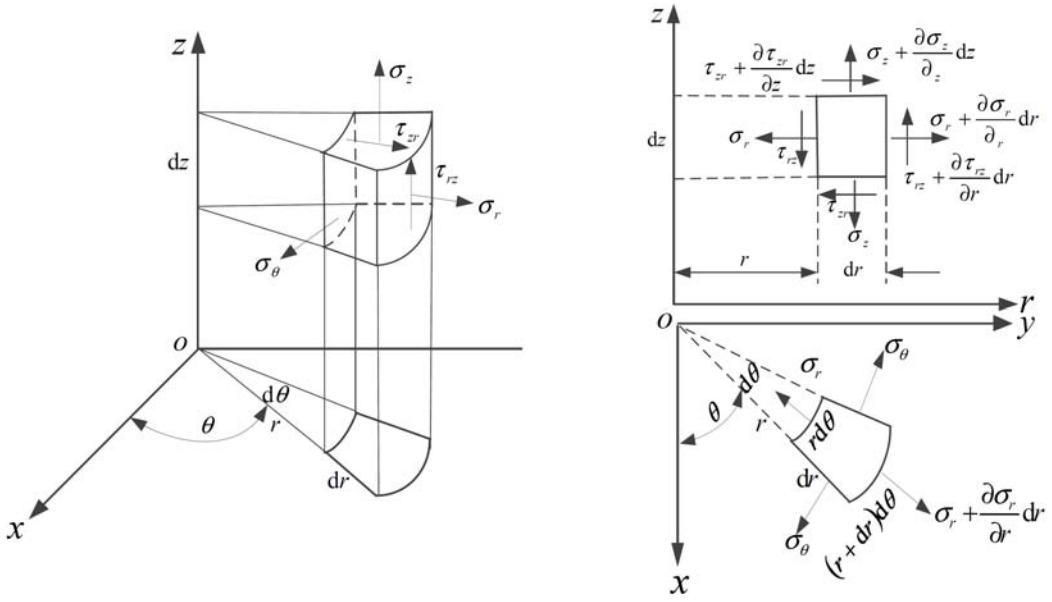

(a) (b)

FIG. 3. Mechanical model of a spatial axisymmetric body: (a) micro-element of a space axisymmetric object, (b) micro-element stress of a space axisymmetric object.

The geometrical equations are

$$\left.\begin{aligned} \varepsilon_r &= \frac{\partial u}{\partial r}, \quad \varepsilon_\theta = \frac{u}{r} \\ \varepsilon_z &= \frac{\partial \omega}{\partial r}, \quad \gamma_{zr} = \frac{\partial \omega}{\partial r} + \frac{\partial u}{\partial r} \end{aligned}\right\}. \tag{2}$$

Among these equations, u、ω are displacement along the direction x and z direction, respectively. In order to obtain the strain–stress relationship of the symmetric thermoelastic body, the linear thermal stress theory was used. The strain is partly caused by stress and partly caused by changes in temperature. Assuming that temperature t is r function, $t = t(r)$, then, for the isotropic body, $\varepsilon_{r0} = \varepsilon_{r\theta} = \varepsilon_{rz} = \alpha t$, $\gamma_{zr0} = 0$. Thus, the total stress is becomes

$$\left.\begin{aligned} \sigma_r &= \frac{E}{(+\mu)}\left[\frac{-\mu}{-\mu}\frac{\partial u}{\partial r} + \frac{\mu}{-\mu}\left(\frac{u}{r} + \frac{\partial \omega}{\partial z}\right)\right] - \frac{\alpha E}{-\mu} \\ \sigma_\theta &= \frac{E}{(+\mu)}\left[\frac{-\mu}{-\mu}\frac{u}{r} + \frac{\mu}{-\mu}\left(\frac{\partial \omega}{\partial z} + \frac{\partial u}{\partial r}\right)\right] - \frac{\alpha E}{-\mu} \\ \sigma_z &= \frac{E}{(+\mu)}\left[\frac{-\mu}{-\mu}\frac{\partial \omega}{\partial z} + \frac{\mu}{-\mu}\left(\frac{\partial u}{\partial r} + \frac{u}{r}\right)\right] - \frac{\alpha E}{-\mu} \\ \tau_{zr} &= \frac{E}{(+\mu)}\left(\frac{\partial \omega}{\partial r} + \frac{\partial u}{\partial z}\right) \end{aligned}\right\}, \tag{3}$$

where μ is Poisson's ratio, E is elastic modulus, and α is linear expansion coefficient. The thermal refocusing model was considered a two-dimensional plane problem. It was assumed in the thermal refocusing system that the inner

diameter is r_i, the outer diameter is r_e, the axial distance is z, one part of the cylinder is fixed [15], and the other part is free without external force.

Apply Eq. (3) to Eq. (1), and Eq. (4) is obtained:

$$G\frac{-\mu}{-\mu}\frac{\partial}{\partial r}\frac{u}{}+\ G\frac{\mu}{-\mu}\left(\frac{}{r}\frac{\partial u}{\partial r}-\frac{u}{r}\right)-\frac{\alpha t}{-\mu}\frac{\partial t}{\partial r}+\ G\left(\frac{}{r}\frac{\partial u}{\partial r}-\frac{u}{r}\right)= \quad . \tag{4}$$

Equation (5) can be derived from Eqs. (4) and (3):

$$\left.\begin{aligned}
\sigma_r &= -\frac{E}{-\mu}\frac{\alpha}{r}\int_{r_i}^{r} tr\ r+\frac{E}{(+\mu)\ -\ \mu}C-\frac{E}{+\mu}\frac{C}{r}+\frac{E\mu}{(+\mu)\ -\ \mu}k\\
\sigma_\theta &= \frac{E}{-\mu}\frac{\alpha}{r}\int_{r_i}^{r} tr\ r+\frac{E}{(+\mu)\ -\ \mu}C+\frac{E}{+\mu}\frac{C}{r}\ -\frac{E\alpha t}{-\mu}+\frac{E\mu}{(+\mu)\ -\ \mu}k\\
\sigma_z &= \frac{E\mu}{(+\mu)\ -\ \mu}C-\frac{E\alpha t}{-\mu}+\frac{E\mu}{(+\mu)\ -\ \mu}k\\
\tau_{zr} &=
\end{aligned}\right\}. \tag{5}$$

C_1, C_2 can be calculated according to the boundary conditions when $r = r_i$ and $r = r_e$; then, $\sigma_r = 0$, such as

$$\left.\begin{aligned}
C\ &= \frac{(+\mu)(\ -\ \mu)}{-\mu}\frac{\alpha}{r_e\ -r_i}\int_{r_i}^{r_e} tr\ r-\mu k\\
C\ &= \frac{+\mu}{-\mu}\frac{\alpha r_i}{r_e\ -r_i}\int_{r_i}^{r_e} tr\ r
\end{aligned}\right\}. \tag{6}$$

Substituting Eq. (6) into Eq. (4), we obtain Eq. (7):

$$\left.\begin{aligned}
\sigma_r &= \frac{\alpha E}{-\mu}\left[-\frac{}{r}\int_{r_i}^{r_e} tr\ r+\frac{r\ -r_i}{r\ \left(r_e\ -r_i\right)}\right]\int_{r_i}^{r_e} tr\ r\\
\sigma_\theta &= \frac{\alpha E}{-\mu}\left[\frac{}{r}\int_{r_i}^{r_e} tr\ r+\frac{r\ +r_i}{r\ \left(r_e\ -r_i\right)}\int_{r_i}^{r_e} tr\ r-t\right]\\
\sigma_z &= \frac{\alpha E}{-\mu}\left(\frac{\mu}{r\ \left(r_e\ -r_i\right)}\int_{r_i}^{r_e} tr\ r-t\right)+Ek
\end{aligned}\right\}. \tag{7}$$

The constant k can be determined by the state of axial force, while displacements u and ω can be derived from Eq. (8):

$$\left.\begin{aligned}
u &= \frac{+\mu}{-\mu}\frac{\alpha}{r}\left[\int_{r_i}^{r} tr\ r+\left(r_i\ +\frac{-\ \mu}{+\mu}r\ \right)\frac{}{r_e\ -r_i}\int_{r_i}^{r_e} tr\ r\right]\\
\omega &= \int^{\omega}\ \omega=\int^{z} k\ z=kz=\frac{\alpha z}{r_e\ -r_i}\int_{r_i}^{r_e} tr-\frac{-\mu}{+\mu}t\quad r
\end{aligned}\right\}. \tag{8}$$

Equation (8) is the mathematical model used for thermal refocusing. The function is the relationship between refocusing compensations u and ω, as well as between structure diameter r, length z, and temperature variation t. Through optical analysis, we can see that the axial displacement ω is the main factor affecting defocusing, and the radial displacement u can be ignored.

The optical calculation amount for focusing is ω = ±0.008 mm, the tilt is less than 15″, and 20 ℃ is the working temperature environment of the space camera. Considering the influence of the space environment, the installation and other nonlinear factors of the camera, the refocusing distance ω was finally determined to be 0.01 mm, so when the ω = ±0.01 mm, α = 22.7 × 10^{-6} ℃$^{-1}$, then we can solve the structure diameter r, length z and temperature variation t. Therefore, according to Eq. (8), the system was developed by optimizing, and the parameters are r_i = 24 mm, r_e = 30 mm, and z = 50 mm . Then, we will verify the reliability of the refocusing system mathematical model through simulation.

3.3. Formatting of Mathematical Components

An optical–mechanical–thermal integrated analysis was conducted for the thermal refocusing system [16], which analyzed the thermal deformation consistency between the refocusing system and the mathematical model with temperature changes by 15 ℃. We calculated the root mean square (RMS) and the secondary mirror shape was obtained by Zernike polynomial fitting [16]. Figure 4(a) shows that the deformation of the refocusing system along the Z-axis is about 0.011 mm, while the second mirror Z-axis is about 0.0101 mm, as shown in Fig. 4(b). Figure 4(c) shows that X-axis deformation is about 6e^{-6} mm, and the MTF is shown in Fig. 4(d).

Focal compensation is realized by thermal deformation, which is likely to cause deformation in the mirror's surface shape and degradation of image quality. The secondary mirror surface figure error plot is extracted by simulation, as shown in Fig. 5. By calculation, the RMS of the mirror is 3.2 nm, which is less than the value of tolerance analysis, *i.e.*, RMS < λ / 50 (λ = 632.8 nm). The Zernike coefficient is obtained by the least square method [17], then the MTF was performed with Zemax optical design software, and there was no obvious change.

By analyzing the data, we found that the deformation Z-axis is close to the calculation results of the mathematical model with an error of about 1%, when comparing the simulation value 0.0101 mm with the design value 0.01 mm. However, the error can be ignored, and the deformation in the radial r direction is small and can also be ignored. The RMS value of the secondary mirror is within the range of optical requirements. Thus, these data verify the accuracy of the mathematical model and the stability of the system. In order to further verify the reliability of the system, we carried out a ground verification experiment for the thermal refocusing system.

IV. EXPERIMENT VERIFICATION

4.1. Ground Verification

The purpose of the experiment was to verify whether the deformation and tilt of the thermal refocusing system coincided with the design requirements under a thermal load. First, the production and assembly of the system were completed, and the plane mirror was pasted on the second-

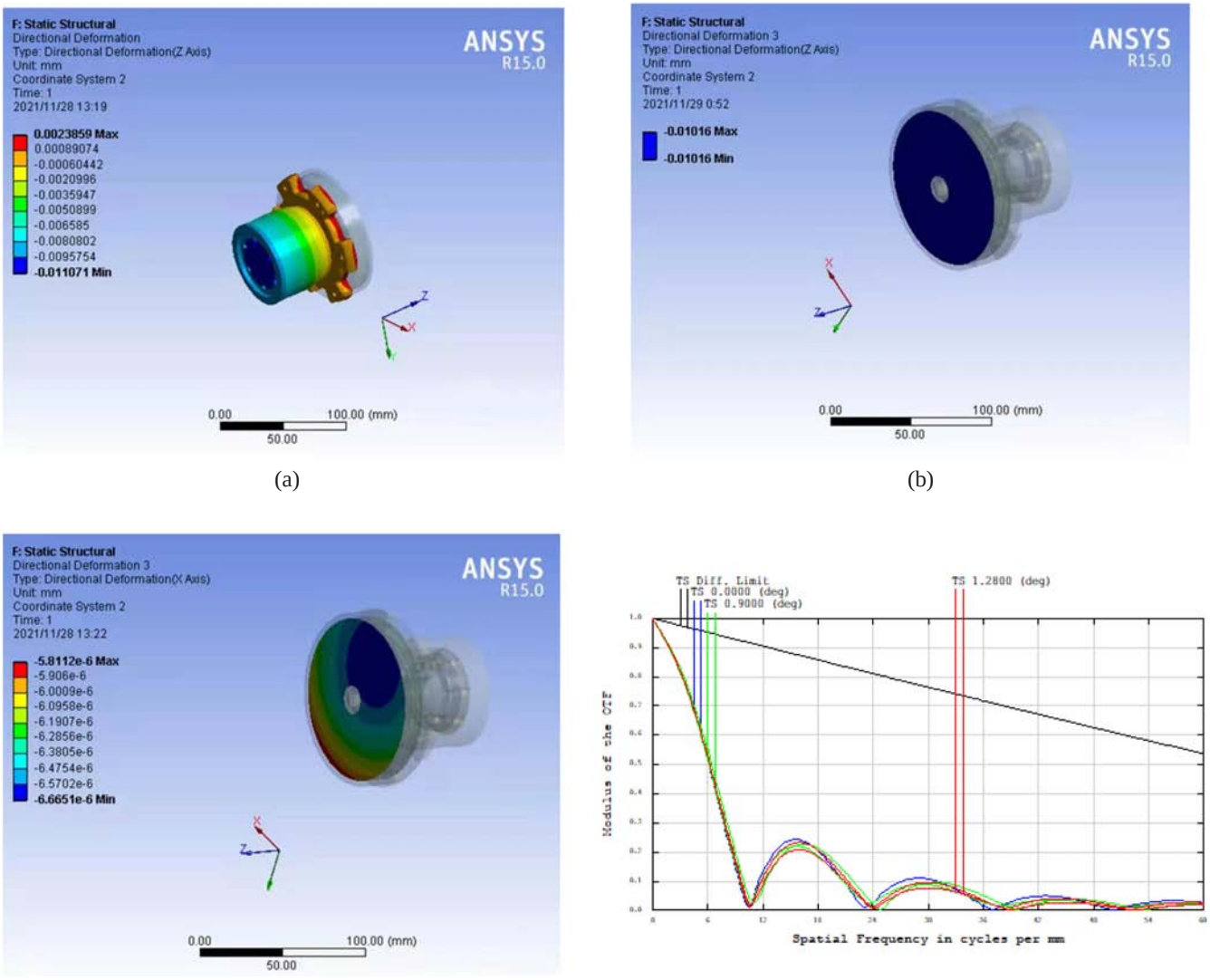

FIG. 4. Influence of the thermal refocusing system: (a) Z-Axis deformation of the thermal refocusing system, (b) Z-Axis deformation of mirror surface, (c) X-Axis deformation of mirror surface, and (d) modulation transfer function (MTF) while the Z-Axis deformation is 0.0101 mm.

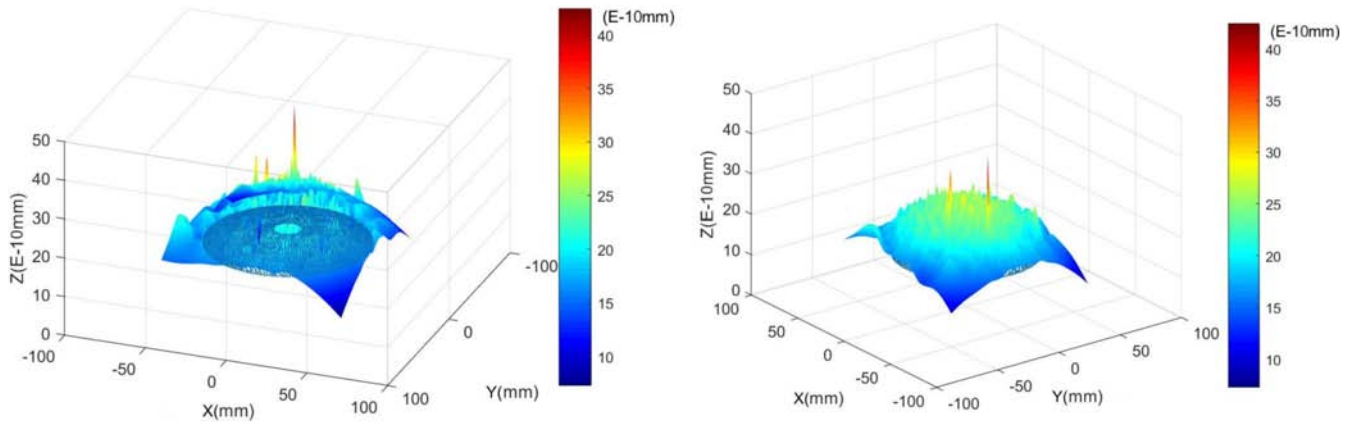

FIG. 5. Secondary mirror surface figure error plot.

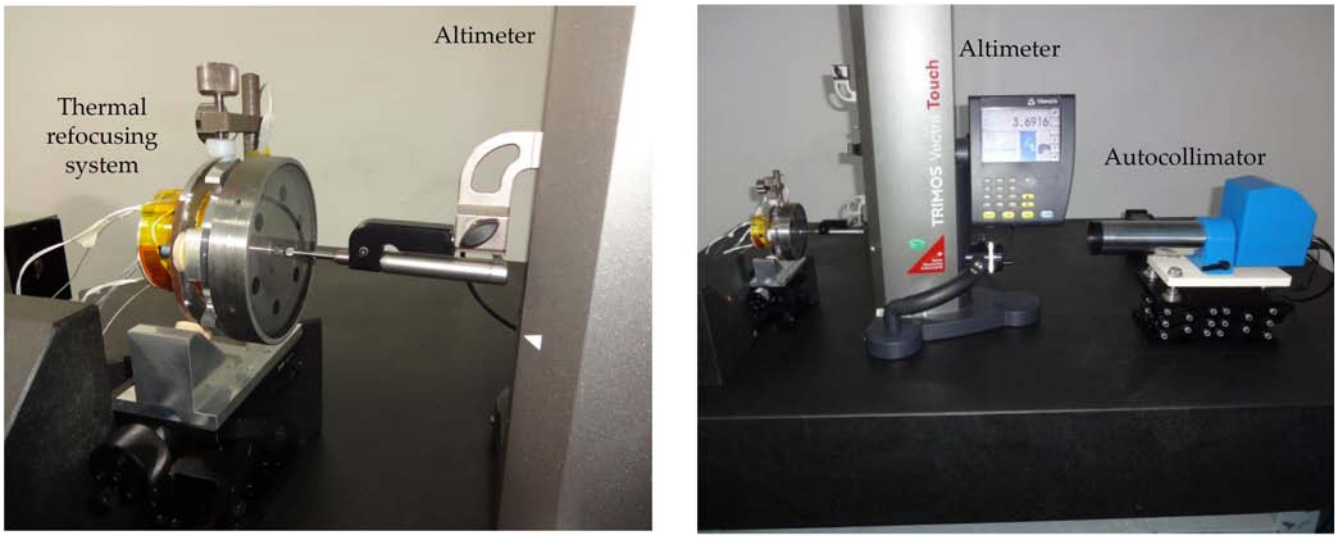

(a) (b)

FIG. 6. Ground experiment of the thermal refocusing system: (a) altimeter measuring displacement and (b) field experiment of thermal refocusing system.

TABLE 4. Results of experimental verification

Number	Temperature (°C)	Displacement (mm)	Tilt X (″)	Tilt Y (″)
1	22.7	3.6936	0	0
2	24.7	3.6921	3.30	4.47
3	27.1	3.6903	5.48	7.00
4	29.5	3.6887	7.13	8.88
5	31.7	3.6875	8.64	9.15
6	34.1	3.6864	9.61	10.53
7	35.7	3.6851	11.54	13.32
8	38.5	3.6839	14.28	13.35

ary mirror and used as an azimuth reference. The inductance probe of the altimeter was hit to the central position of the plane mirror to measure its displacement. The normal direction of the plane mirror was obtained by using a CCD biaxial autocollimator to measure the tilt of the refocusing system [18]. The test is shown in Fig. 6.

During the experiment, the thermal resistance measured the initial temperature of the refocusing system at 22.7 ℃. The position of the altimeter and the autocollimator was adjusted to ensure that the angle value of the autocollimator in two directions was 0, which was used as the initial state for the experiment. The aluminum ring is heated every 2 ℃ as a step, and data on deformation and tilt in the X direction and Y direction were taken every step. The data were measured three times repeatedly, and are shown in Table 4.

According to the experimental results, when the temperature varies by 15.8 ℃, the displacement is about 0.0097 mm, and the tilt is less than 15″. When analyzing the data, we found that the displacement was less than the simulation

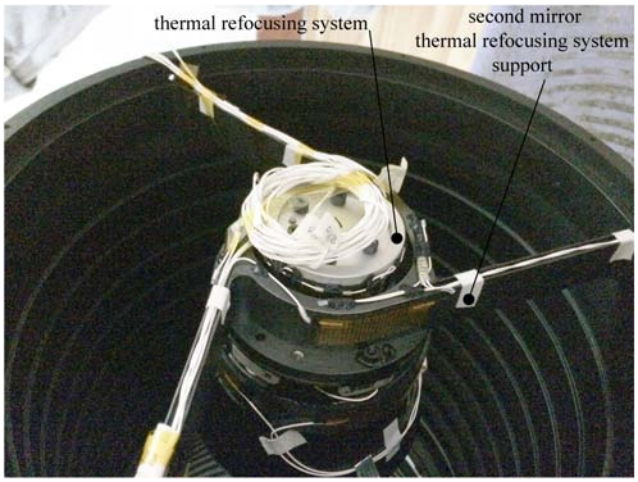

FIG. 7. Completed assembly of the thermal refocusing system.

and mathematical model data, which is due to the influence of the coupling factors in the system. The tilt accuracy met the requirements appropriately. After the ground verification of the thermal focusing system was completed, the camera was assembled, and the position of the secondary mirror is shown in Fig. 7.

4.2. Thermal Vacuum Experimental Verification

In the previous section, we separately verified the reliability of the secondary mirror focusing system, but it was not clear whether the thermal refocusing performance of the system in the whole camera met the design requirements. Therefore, we conducted a thermal vacuum experiment to further verify the reliability of the focusing system in addition to verifying the thermal characteristics of the camera. The experimental site is shown in Fig. 8.

During the verification of the active thermal refocusing system, it was determined that the MTF of the camera reached its highest at 21 ℃. When the temperature of the entire camera remained at 21 ℃, the temperature of other parts of the camera remained unchanged—that is, we only needed to adjust the temperature of the refocusing system, control the image plane position, collect the edge and discrimination target images, test the refocusing range by moving the target position of the collimator, and change the target position, as shown in Table 5. The actual displacement was compared with the theoretical value to verify the reliability of the refocusing system.

By analyzing the above data, we found that the actual displacement was about 0.009 mm, while the temperature varied by 13.9 ℃. There was a slight difference in the design during the refocusing experiment, mainly due to the accuracy of temperature control and test temperature components, but it was within a controllable range. It can be seen in Fig. 9 that the MTF with refocus is significantly improved compared to that without refocus. For example, at about 8 ℃, the MTF of the camera without refocus is 0.08, while the MTF value with refocus is 0.12, which effectively improves the imaging quality by 50%; there was a small error between the theoretical value and the experimental value, but the trend was consistent, which was caused by measuring instrument errors and the influence of nonlinear factors.

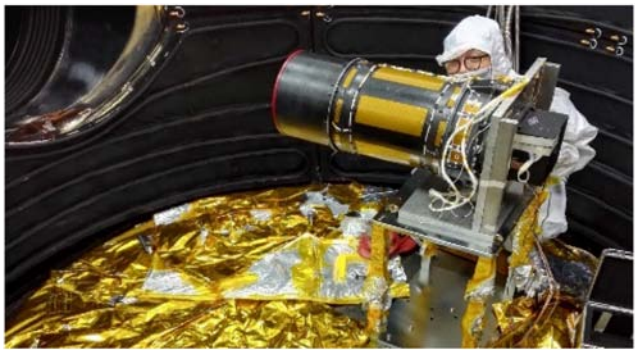

FIG. 8. Thermal vacuum experiment.

TABLE 5. Thermal vacuum experimental data

Design Temperature (°C)	Actual Temperature (°C)	Without Refocus MTF	Actual Displacement (mm)	With Refocus MTF
7	7.1	0.07	0.0013	0.12
9	8.8	0.08	0.0013	0.12
11	11.2	0.09	0.0012	0.12
13	13.1	0.09	0.0011	0.13
15	14.9	0.11	0.0013	0.13
17	17.0	0.12	0.0012	0.13
19	19.2	0.12	0.0015	0.13
21	21.0	0.13	0	0.13
23	22.9	0.12	0.0011	0.13
25	25.1	0.11	0.0012	0.13
27	27.2	0.11	0.0013	0.13
29	29.1	0.09	0.0011	0.13
31	30.8	0.08	0.0011	0.12
33	32.9	0.08	0.0009	0.12
35	35.0	0.05	0.0013	0.12

4.3. In-orbit Verification

The CX6-02 satellite was successfully launched and good images were obtained. For example, Fig. 10 shows the camera's in-orbit images: Fig. 10(a) is a target. After the launch of the space camera, the ground resolution was tested through the ground target. Through ground data processing, it was verified that the resolution of the camera reaches 1.4 m, meets the optical requirements, and obtains good images, as shown in Fig. 10(b) which presents the Beijing national stadium (bird's nest), Beijing national aquatics center (water cube), and the surrounding area of Beijing. The image quality is good and meets the requirements of the optical system. Moreover, the stability and reliability of the refocusing system were verified.

V. CONCLUSION

In order to further research the thermal refocusing system of a high-resolution camera, the development of a CX6-02 was used as an example. We established a mathematical model of the thermal refocusing system based on thermoelasticity, and we verified the model's accuracy by using optical–mechanical–thermal integration simulation analysis, a ground experiment, and an in-orbit image. All the verification data show:

1) There was about a 1% error between the thermal refocusing system mathematical model and optical–mechanical–thermal integration simulation; the model's displacement was 0.01 mm while the simulation's displacement was 0.0101mm. The ground experiment displacement was 0.097 mm and the thermal vacuum experiment displacement was 0.089 mm. These results were primarily caused by the superposition and coupling effect of multiple

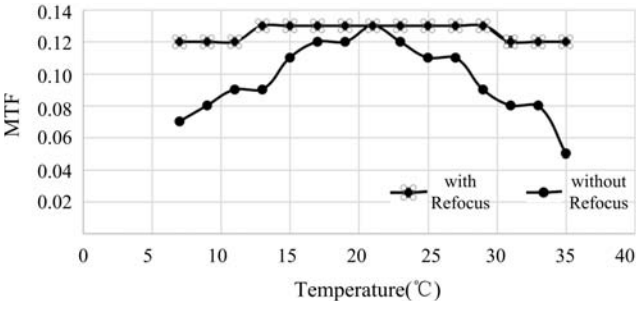

FIG. 9. Temperature-MTF relation chart.

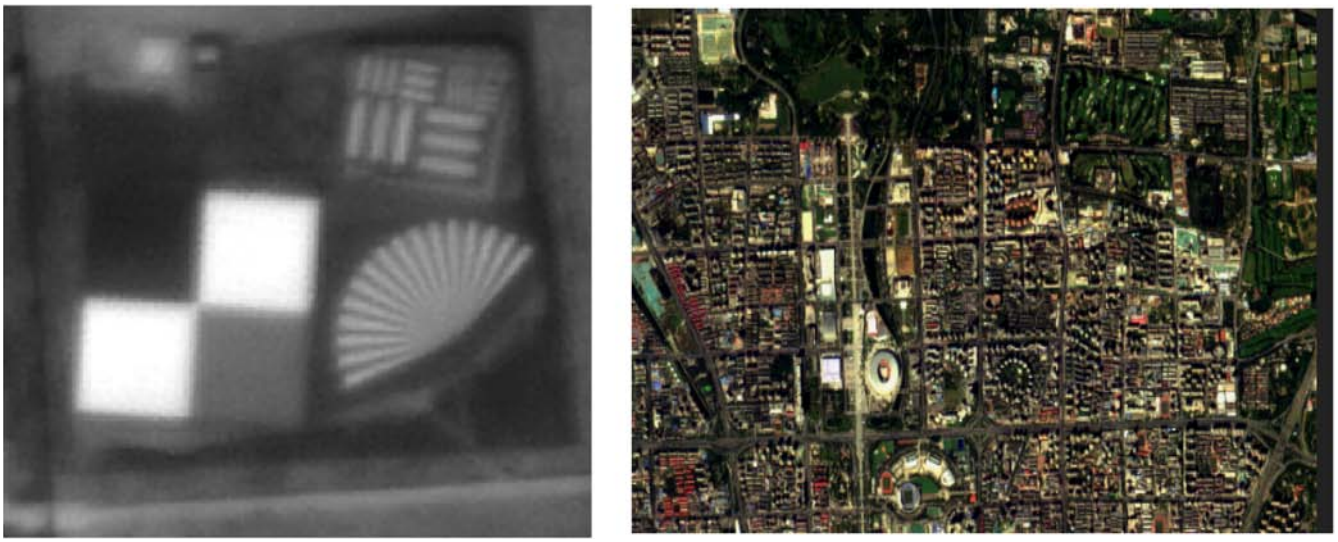

(a) (b)

FIG. 10. In-orbit images of CX6-02 satellite: (a) target, (b) Beijing national stadium (bird's nest) and Beijing national aquatics center (water cube).

structures, but did not affect the function of the system and can be ignored.

2) The RMS value of the mirror surface of the thermal refocusing system of the secondary mirror was obtained by a Zernike fitting calculation, which met the requirements of the optical index and indicated the stability of the focusing system.
3) The in-orbit image was excellent, and it showed that the thermal refocusing system had good stability and high precision.

In summary, the mathematical model of the thermal refocusing system is consistent with the simulation and experimental verification. It provides a theoretical and practical basis for the thermal control focusing of a high-resolution space camera and has great adaptability and broad application prospects.

ACKNOWLEDGMENT

This study was supported by the National Natural Science Foundation of China (61635002) and "Hyperspectral video stereo imaging for environment perception of unmanned vehicles (2020-JCJQ-JJ-492)."

DISCLOSURES

The authors declare no conflict of interest.

REFERENCES

1. Y.-L. Ding, H.-Y. Tian, and J.-Q. Wang, "Design on the focusing mechanism of space remote-sensing camera," Opt. Precis. Eng. **9**, 35–38 (2001).
2. F. Q. Guo, J. H. Dong, W. Li, K.-J. Wang, Y.-C. Li, and H.-P. Wang, "Focusing mechanism design for long focal length space camera," OME Inform. **11**, 105–109 (2010).
3. H. P. Huang, Y. H. Xia, C. B. An, and X. D. Zhang, "Design on the focusing mechanism of long focus IR system," Laser Infrared **35**, 745–747 (2005).
4. Q. P. Cao, Z. Ye, X. J. Dong, H. Yin, and J. Zhu, "Method of focusing of foreign space camera based on image evaluation," Laser Optoelectron. Prog. **52**, 011102 (2015).
5. D. Korsch, "Closed form solution for three-mirror telescopes, corrected for spherical aberration, coma, astigmatism, and field curvature," Appl. Opt. **11**, 2986–2987 (1972).
6. O. Selımoglu, M. Ekinci, and O. Karcı, "Thermal refocusing method for spaceborne high-resolution optical imagers," Appl. Opt. **55**, 4109–4112 (2016).
7. A. S. McEwen, E. M. Eliason, J. W. Bergstrom, N. T. Bridges, C. J. Hansen, W. A. Delamere, J. A. Grant, V. C. Gulick, K. E. Herkenhoff, L. Keszthelyi, R. K. Kirk, M. T. Mellon, S. W. Squyres, N. Thomas, and C. M. Weitz, "Mars reconnaissance orbiter's high resolution imaging science experiment (HiRISE)," J. Geophys. Res. **112**, E05S02 (2007).
8. P. Verhoeff, H. A. van Mierlo, B. C. Braam, J. C. W. Hopman, W. P. van Werkhoven, and M. Le Kluse, "Development of an in-orbit refocusing mechanism for the Meteosat second generation weather satellites," Proc. SPIE **3439**, 92–103 (1998).
9. H. Shibai, "ASTRO-F mission," Proc. SPIE **4850**, 162–169 (2003).
10. J. L. Lamard, "Design of the high resolution optical instrument for the Pleiades HR earth observation satellites," in *Proc. 5th International Conference on Space Optics* (Toulouse, France, Jun. 2004), pp. 149–156.
11. C. Miravet, D. Zorita, J. I. Bueno, L. Pascual, A. García Marín, G. Taubmann, J. Azcona, J. M. Arroyo, I. Monasterio, U. García, J. Martin, C. Mas, J. Muñoz, A. Lopez, J. Eguía, S. Jarabo, R. García, R. Navarro, T. Belenguer, L. M. González,

C. Pastor, D. Arrazola, C. Gonzalez Alvarado, I. Cabeza, A. Borges, A. Marini, and G. Crippa, "Development status of the telescope for the Ingenio/SEOSAT mission primary payload," Proc. SPIE **8167**, 816711 (2011).
12. P. Hartmann, K. Nattermann, T. Döhring, M. Kuhr, P. Thomas, G. Kling, P. Gath, and S. Lucarelli, "ZERODUR glass ceramics: strength data for the design of structures with high mechanical stress," Proc. SPIE **7018**, 70180P (2008).
13. Q. X. Li, D. S. Wang, and Y. H. Li, *Design of modern precision instruments* (Tsinghua University Press, Beijing, China. 2009).
14. Z. L. Xu, *Elasticity* (Higher Education Press, Beijing, China. 2020).
15. J. Huang, Y. Wang, J. Zeng, H. Yu, X. Wu, L. Lu, X. Li, and X. Zhang, "Optical fiber monitoring technology for thermal strain and thermal deformation of spatial deployable mast," Aerospace Shanghai **37**, 70–78 (2020).
16. Y. Xiao, W. Xu, and C. Zhao, "Integrated simulation of optomechanical system," Acta Opt. Sinica **36**, 722002 (2016).
17. J. Yang, W. Huang, and Y. M. Han, "Application and simulation in fitting optical surface with Zernike polynomia," Spacecr. Recovery Remote Sens. **31**, 49–55 (2010).
18. X. J. Zhang, C. X. Yan, and T. Xie, "Design of focusing mechanism of space remote sensor," Opt. Precision Eng. **17**, 2757–2761 (2009).